Response to Reviewer-1

Review of: Global Monsoon in ICON: The scale-dependent response of Northern Hemisphere Monsoons

Authors: Praveen Kumar Pothapakula*, Andreas F. Prein, Anusha Sunkisala, and Anurag Dipankar

Journal: Weather and Climate Dynamics

Review: The authors are examining the fidelity of the ICOsahedral Non-hydrostatic (ICON) model in simulating the hydroclimate of the various regional monsoons in the tropics. They use a 10 year atmosphere-only simulation forced with observed SST to assess the model simulation of the seasonal cycle, interannual, intraseasonal variations and extreme rain events.

Overall the paper is well written and the figures are of high quality. I consider this paper to be important as it is familiarizing the readers with a relatively new model on its performance of the monsoon. The paper is easy to read and understand and I would support its publication after the authors address the following comments:

We thank the reviewer for the encouraging comments and for their constructive questions, which ranged from fundamental scientific arguments to helpful suggestions for improving the description of the datasets. We have now addressed all the comments with additional figures, analysis, and detailed reasoning. Please find our point-by-point responses below.

1. At the tested spatial grid spacings of 80, 40, and 10km don't believe that the nonhydrostatic feature is important at all. So, my question then is what is the purpose of running an expensive feature like the non-hydrostatic option for this study at all?

Thank you for raising this fundamental and very important question.

- We kindly refer to Liu et al. (2022), who investigated the non-hydrostatic (NH) vs. hydrostatic (H) dynamical core performance using the Simple Cloud-Resolving E3SM Atmosphere Model (SCREAM) at grid spacings from ~30 km to 10 km, with real-world experiments. E3SM, like ICON, uses an irregular grid and is a next-generation global modeling system. Their results revealed significant NH vs. H differences in the tropics, particularly over India, the Pacific Ocean, and the Indian monsoon core region (we refer to Fig.1 of Liu et al. (2022)). Even at 30 km resolution, the NH dycore produced 20% more rainfall over the Indian monsoon core compared to the H dycore, demonstrating that NH dynamics help reduce the dry bias over central India even at relatively coarse resolution. Liu et al. attributed this difference to changes in vertical velocity fields rather than surface moisture

- Motivated by these findings, we analyzed vertical velocity (w) across our three resolutions (80, 40, and 10 km) over the monsoon core regions. Our results (Fig. 1) show that updrafts are systematically stronger at finer grid spacing (10 km > 40 km > 80 km). Furthermore, these

stronger updrafts enhance the conversion of cloud water (qc) to rain water (qr), producing more precipitation (see response to comment #5). These results are consistent with Liu et al. (2022).

- Our experimental design (NH at all resolutions, grid spacing varying) does not allow us to separate the effects of grid spacing from those of NH dynamics. We therefore do not claim to have isolated the NH contribution. The detailed effects of NH vs. H are beyond the scope of this paper.

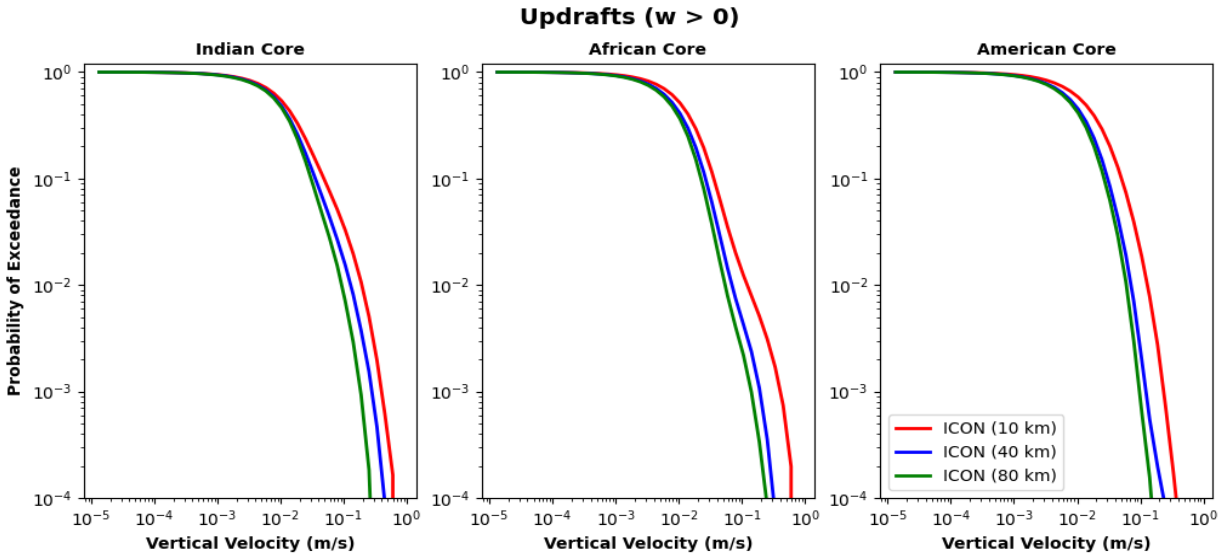

Figure 1: Vertical velocity (w) cumulative distribution function, or probability of exceedance on a logarithmic probability scale for various ICON simulations over the SAsiaM, NAfriM and NAmerM core monsoon regions at 850hPa level. The probability of exceedance plot highlights the intense updrafts with changing horizontal grid spacings. All the simulations are analysed at a common 30 km grid for fair comparison.

2. The tracks of the low pressure systems in Fig. 12 suggest that the results in the paper are representative of the 10-year integration period (2006-16) of ICON or sensitive to the algorithm used to diagnose these systems. For instance, Vishnu et al. (2020; https://doi.org/10.1029/2020JD032977) also find a fair number of tracks going northward towards Bangladesh from northern head Bay of Bengal as opposed to just northwestward tracks. So could you comment on this?

We thank the reviewer for this observation. To clarify whether the track characteristics in Fig. 12 of the manuscript are sensitive to (a) the 10-year integration period or (b) our in-house tracking algorithm, we conducted a series of sensitivity tests.

Specifically, we tested a range of sea-level pressure thresholds (ΔSLP = 2-4 hPa) and maximum linking distances (150-250 km), encompassing and extending the values used in Vishnu et al. (2020). Here, ΔSLP is the pressure threshold relative to the local minimum used to define a low-pressure system, and linking distance is the maximum distance a system is allowed to move within 6 hours while still being considered the same storm. These values were chosen to assess whether reducing the linking distance would preferentially capture shorter, northward-propagating tracks from the head of the Bay of Bengal toward Bangladesh.

From these sensitivity tests, we found that while the total number of detected systems changes slightly, the overall spatial structure of the tracks, including the dominant northwestward propagation remains largely unchanged (Fig. 2). This indicates that the track orientation is not strongly sensitive to the specific parameter choices in our tracking algorithm.

The differences relative to Vishnu et al. (2020) are therefore more likely related to differences in the analysis period and dataset characteristics. Vishnu et al. (2020) derived their results from multi-decadal reanalysis datasets (1979–2019), which provide a climatological representation of LPS behavior. In contrast, our analysis is based on a shorter 10-year period (2006–2016), which may not fully capture the full range of interannual variability in track pathways. It is well known that LPS propagation is modulated by large-scale monsoon conditions and can vary substantially from year to year, a shorter sampling period may under-represent less frequent track types, such as northward-moving systems toward Bangladesh. Consistent with this interpretation, we observe from the IMD best track data that very few LPS propagate toward Bangladesh during our study period.

Overall, our analysis confirms that the algorithm parameter choices do not fundamentally alter the spatial structure of the detected tracks. We therefore conclude that the differences relative to Vishnu et al. (2020), particularly the absence of northward-propagating tracks toward Bangladesh are more likely attributable to sampling variability and interannual variability in LPS pathways, rather than to methodological inconsistencies in the tracking algorithm.

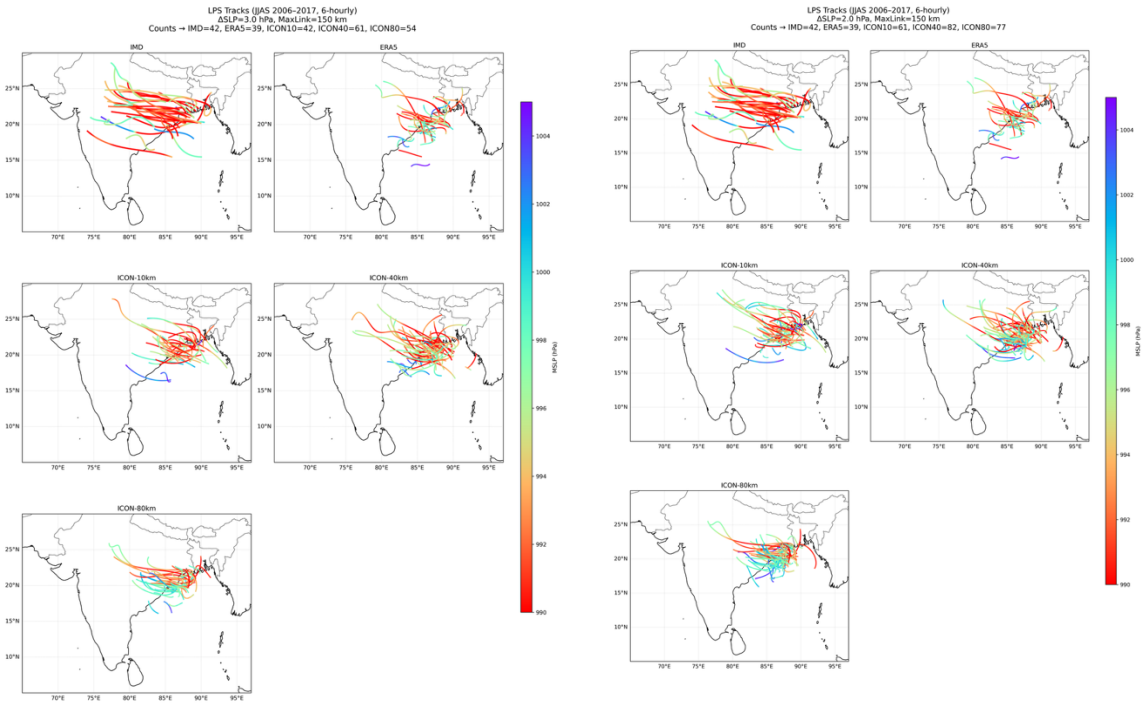

Figure 2 : Sensitivity tests with LPS tracking algorithm to test for tracks passing India and Bangladesh (left) by reducing the linking distance between two points on a track (right) changing the ΔSLP and fixing the linking distance to 150 km.

3. If the authors wish to compare the results with a variety of precipitation observations then they should also summarize their merits and disadvantages.

We appreciate the reviewer for pointing out this important information. We have now added relevant information discussing the merits and disadvantages of the observational/reanalysis products used in the study. (Appendix A, L715-L748)

- IMERG combines passive microwave estimates from multiple low-earth-orbital satellites with geostationary infrared (IR) observations and gauge data. Sophisticated techniques such as morphing and Kalman filter compensate for the limited low earth orbital sampling, enabling high-temporal (30-min) and spatial resolution. However, this dataset is limited due to its indirect estimation of the infrared channel for filling temporal gaps, and morphing techniques assume linear motion. Furthermore, gauge bias correction at monthly intervals is limited over the ocean, thus enhancing the probability for bias. Despite these limitations, IMERG represents the state-of-the-art in multi-satellite precipitation estimation over the tropics.

- MSWEP data uses a multitude of gauges (76,747 stations), satellites (CMORPH, GSMaP, TMPA), and reanalyses (ERA-Interim, JRA-55) into a global 0.1°, 3-hourly product. It has a full comprehensive land-ocean coverage with discharge-based bias correction (13,762 stations), and improved performance in mountains. Its 3-hourly temporal frequency misses sub-daily extremes, its reliance on gauge stations limits performance in regions of sparse network, discharge correction is indirect, complex methodology has assumptions.

- CMORPH, similar to GPM IMERG, retrieves precipitation from passive microwave sensors deployed on low-earth orbiting satellites, and uses cloud motion vectors from geo-stationary satellites to morph precipitation. The data is also a bias-corrected version against CPC gauges (land) and GPCC (ocean). CMORPH has high temporal resolution, global coverage, and has a good warm-season performance. However, like GMPM, it uses morphing and thus assumes linear motion, has biases in complex terrain, underestimates heavy rain, and has variable regional performance.

- The GPCC provides gridded gauge-based precipitation analyses derived from quality-controlled in-situ station data over global land surfaces based on up to 84,800 stations . This product uses a large station network across the globe and has established quality control procedures (Becker et al., 2013, Schamm et al., 2014, Schneider et al., 2018). However, it is limited by the variable station density and bias correction for systematic gauge measuring errors. ((Becker et al., 2013 (DOI:10.5194/essd-5-71-2013); Schamm et al., 2014 (DOI: 10.5194/essd-6-49-2014); Schneider et al., 2018 (https://opendata.dwd.de/climate_environment/GPCC/PDF/GPCC_intro_products_v2018.pdf))

- The CPC provides gauge based analysis of global daily precipitation over land- and surfaces. It uses optimal interpolation to combine data from over 30,000 rain gauges. It uses relatively large station network, rigorous quality control and provides estimations of gauge counts per grid cell, and acounts for orographic effects during interpolation. Like GPCC, this dataset is also limited by variable station density and has course spatial resolution.

- In addition to observational datasets, we used ERA5 which uses a vast amounts of historical observations (from satellites, radiosondes, aircraft, weather stations, and ships) with a numerical weather prediction model using data assimilation to create a physically consistent, globally complete dataset.

- To validate our low pressure system tracks form ICON, we used IMD best track datsets to estimate the positions at 6 hourly intervals. It uses a multi-satellite approach for locating storm centers such as ndian geostationary satellites (Kalpana-1, INSAT-3A, and later INSAT-3D) along with polar-orbiting satellites from international partners. This dataset however relies completely on satellites, and hence the estimatons are biased especially during intense cloud days.

4. It would be nice to show the topography represented at all three grid resolutions.

- Thank you, we agree that topography is an important figure to show. We have now added this figure to the supplementary material (Fig. S1, zoomed figure in Fig. S2). Furthermore, we have added the discussion on resolution sensitivity in resolving the fine-scale topography in the manuscript. (updated in L141-L144)

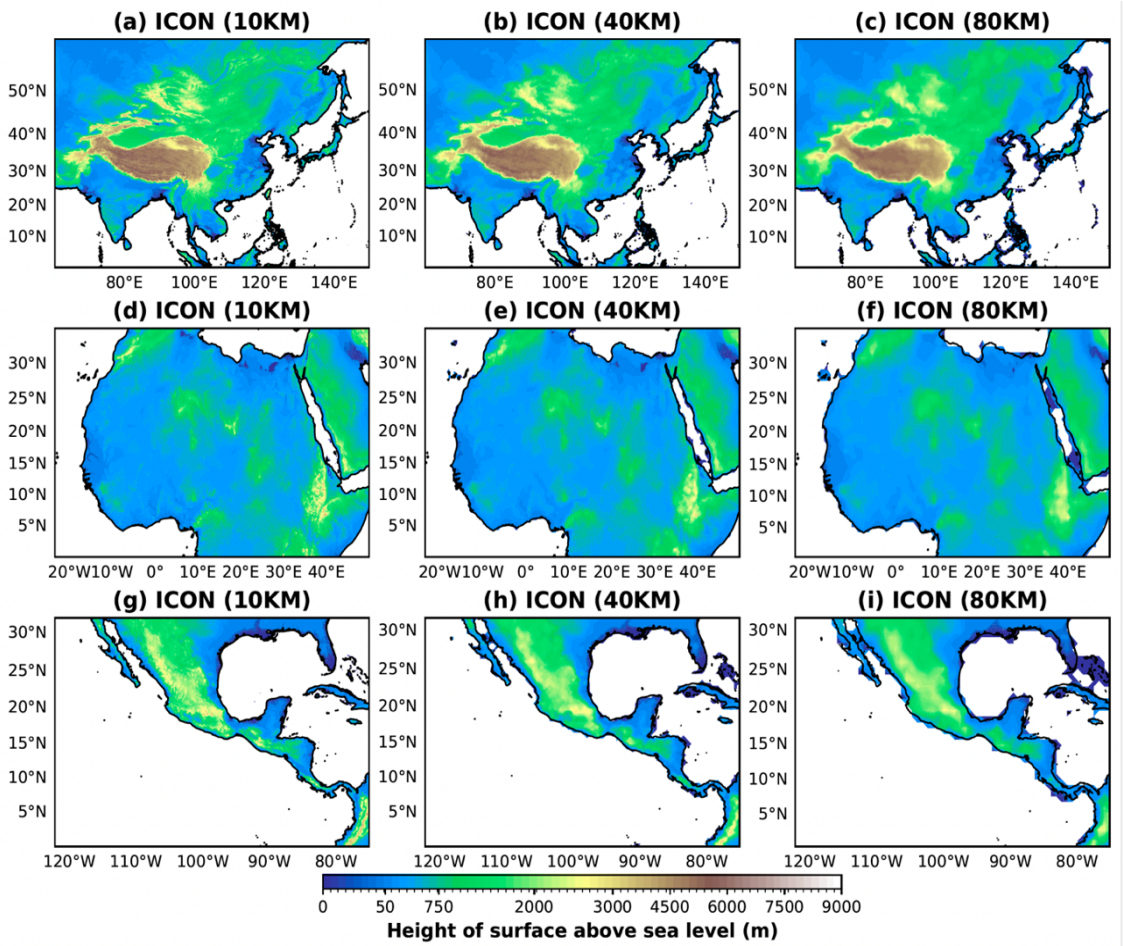

Figure 3 : Topography of Northern Hemisphere monsoon domains in various ICON simulations at 10 km, 40 km, and 80 km grid-spacing. (a-c) SAsiaM domain (d-f) WAfriM domain and (g-h) NAmerM domain

5. I would be curious to know if the partitioning of convective and stratiform precipitation changes across resolutions? Likewise does the fraction of high, medium, and low cloud cover change across resolutions for light, medium, and heavy rain events? Is there a difference in the precipitation efficiency and precipitation recycling ratio across resolutions?

Thank you for the comment. We have now added a detailed explanation, results, and description in the manuscript (L503-L521). Below is our detailed response to this question.

Partitioning of convective and grid-scale (resolved) precipitation: In Fig. 9 of our manuscript, we have shown the probability distribution of total precipitation, and in supplementary material Fig. S11, the distributions of convective precipitation across various simulations and monsoon domains. Our results show that the contribution of convective precipitation, especially for high-intense precipitation events (> 10 mm/day), decreases with decreasing grid spacings, indicating that the difference in the precipitation contributions across simulations is largely due to the resolved grid-scale precipitation.

To further enhance this important point, we have quantified the contribution of convective and grid-scale precipitation to the total precipitation in monsoon core regions across various simulations in the table below (Table 1).

Table 1: Quantification of convective (Vs) grid-scale precipitation

Resolution	South Asia % grid-scale (% conv)	North Africa (% grid-scale)/ (% conv)	North America (% grid-scale)/ (% conv)
10 km	46% (54%)	30% (70%)	10% (90%)
40 km	32% (68%)	16% (84%)	6% (94%)
80 km	28% (72%)	12% (86%)	4% (96%)

These results indicate that fine grid spacing induces more grid-scale precipitation compared to the coarse grid spacing simulation in all three monsoon cores. Notably, over the SAsiaM (28% -> 46%) and NAfriM (12% -> 30%). Correspondingly, the convective fraction decreases. This indicates that higher resolution allows the model to generate more explicitly resolved precipitation, reducing the dominance of parameterized convection. However, it is important to note that the rate of increase in the grid-scale precipitation is not proportional to the decrease in convective precipitation. For example, over South Asia, the 10 km simulation's grid-scale's gain exceeds the convective loss by a factor of 1.7, and 1.5 over Africa. This indicates that fine grid spacing does not merely partition the existing precipitation but generates additional precipitation through explicitly resolved dynamics.

Sensitivity of Cloud Cover to Grid Spacing:

For the whole Monsoon Season (JJAS): Following your suggestion, we show the cloud cover from various ICON simulations on the model levels (120 levels) with corresponding estimated height above the sea level over the monsoon core region in Fig. 4. The results show that over SAsiM and NAfriM , the cloud cover is sensitive to grid spacing, and less so over NAmerM. Particularly, we notice a systematic decrease in the low-level clouds and high-level clouds over these regions, with little impact on mid-level clouds.

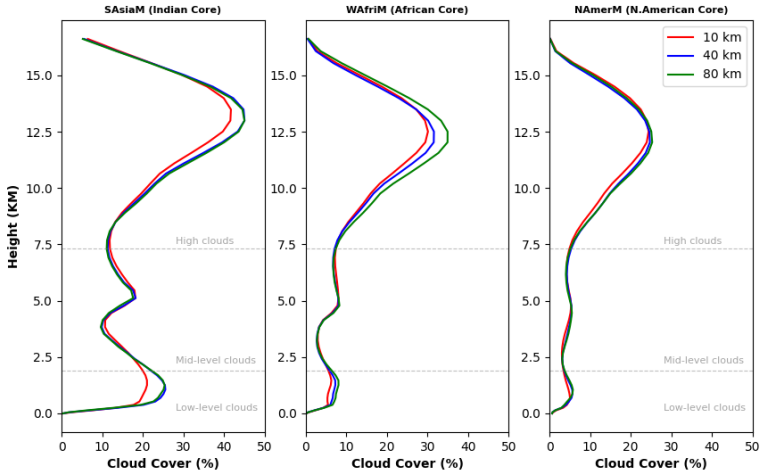

Figure 4: Sensitivity of total cloud cover (%) to grid spacing in ICON 10 km, 40 km, and 80 km simulations for the SAsiaM, WAfriM, and NAmerM domains. The cloud cover is averaged over the respective monsoon core regions and is plotted against model levels converted to height above sea level.

Extreme Events Cloud Cover: Investigating further into the cloud cover distribution over the core monsoon regions during intense precipitation events (median precipitation over core monsoon region > 5 mm/day) shows similar behavior of the average cloud distribution during the entire monsoon season, with the exception of NAmerM high clouds (Fig. 5).

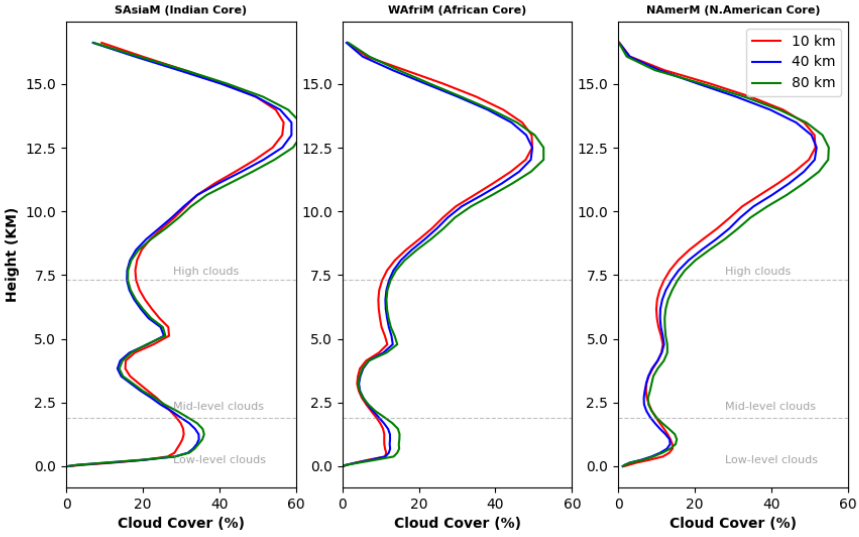

Figure 5: Same as Fig. 4, but for extreme precipitation event days over the Monsoon core regions.

Moderate Events Cloud Cover: For the moderate precipitation days (median precipitation over the core monsoon region > 2 mm/day and < 5 mm/day), the low-level clouds consistently decrease with fine grid spacing, while the mid-level clouds show a slight increase in fine grid spacing in SAsiaM and NAfriM core monsoon region (Fig. 6).

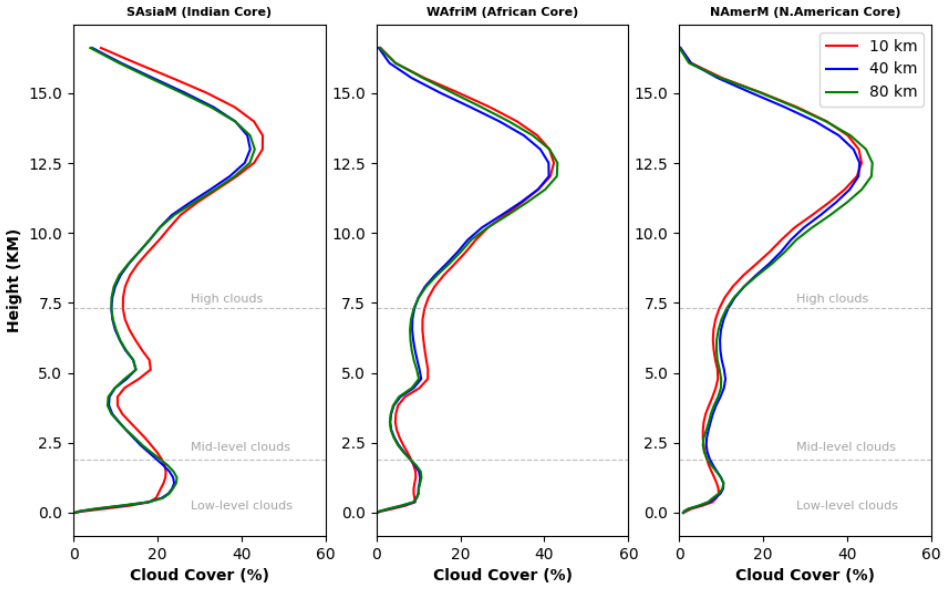

Figure 6: Same as Fig. 4, but for moderate precipitation event days over the Monsoon core regions.

Light Rain Event cloud Cover: Only over SAsiaM, the mid and high-level clouds are sensitive to the grid spacing during light rain days, however, the percentage contribution of these clouds is less than the medium and intense precipitation days (Fig. 7).

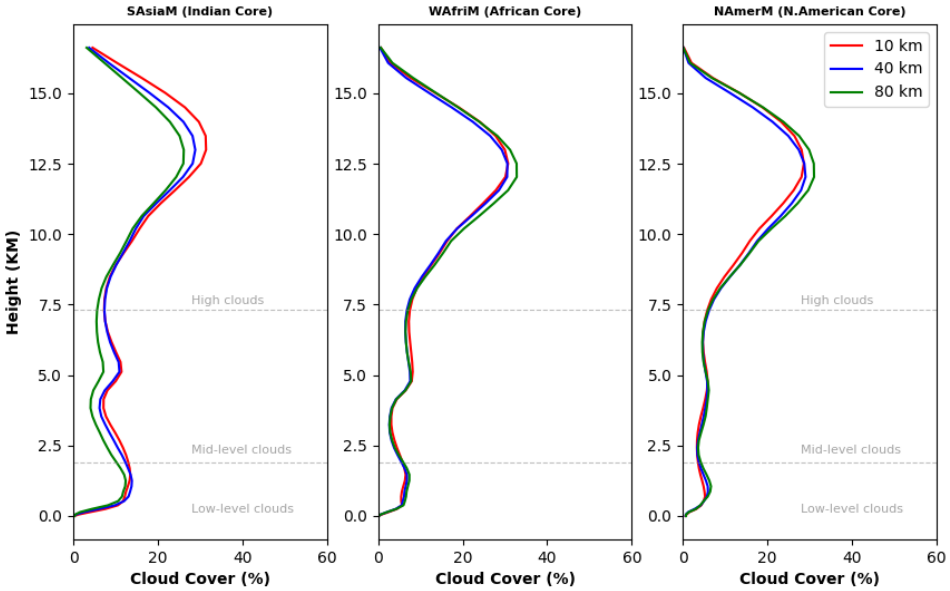

Figure 7: Same as Fig. 4, but for light precipitation event days over the Monsoon core regions.

Overall, the results indicate that the fine grid spacing results in decreased cloud cover, especially the low-level clouds and the high-level clouds during intense and moderate rainy days. The cloud cover over the SAsiaM and NAfriM monsoon core regions is sensitive to grid spacing compared to NAmerM domain. The results are consistent with the previous studies, i.e., clouds become smaller and smaller with decreasing grid spacing (Langhans et al., 2012a, Prein et al., 2015).

Precipitation efficiency and precipitation recycling ratio: Here, we distinguish precipitation efficiency between cloud microphysics and the boundary layer, presenting results from two perspectives. Furthermore, we plan to investigate a detailed water budget analysis in a future

study; for this review, we use simple metrics to provide preliminary insights into these processes.

(a) Rain conversion in microphysics: We plot the prognostic variables, cloud water content (kg/kg) and rain water content (kg/kg) on model pressure levels (Fig. 8 and Fig. 9). Unfortunately, these variables are not saved on native model levels, so smooth vertical profiles are not expected due to interpolation onto limited pressure levels. The results indicate that cloud water content decreases in the mid-tropospheric levels with finer grid spacing over SAsiaM and NAfriM, while the results are less sensitive over NAmerM. We focus on mid-tropospheric properties as they are crucial for rain formation processes. Furthermore, across all simulations, rain water content increases with finer grid spacing, indicating that fine grid simulations more efficiently convert available cloud water into warm rain. A systematic increase in vertical velocity with finer grid spacing can enhance collision-coalescence and riming processes, thus leading to increased precipitation. Therefore, finer grid spacing enhances precipitation efficiency at the cloud microphysical scale.

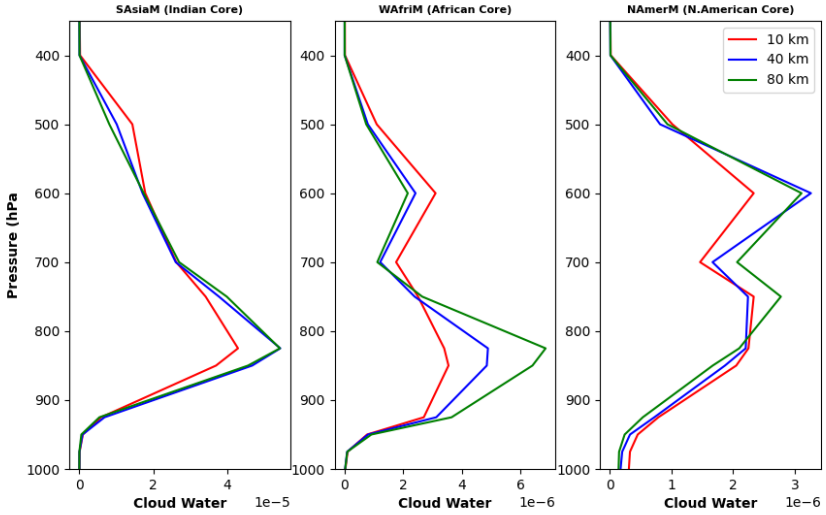

Figure 8: Sensitivity of cloud water (kg/kg) to grid spacing in ICON 10 km, 40 km, and 80 km simulations for the SAsiaM, WAfriM, and NAmerM domains. The cloud water is averaged over the respective monsoon core regions and is plotted against pressure levels level.

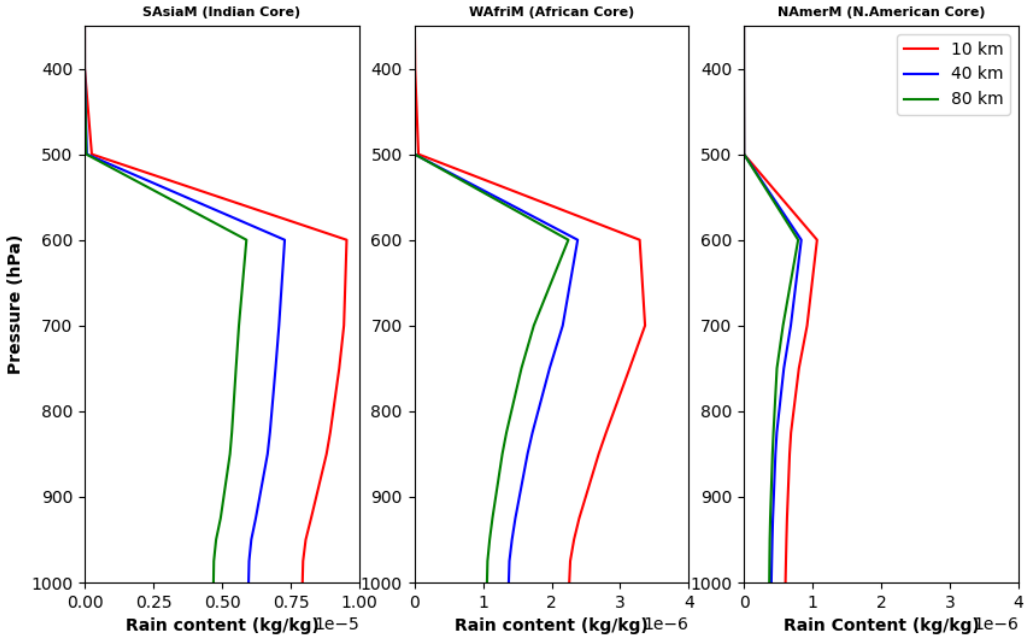

Figure 9: Same as Fig.8, but for rain content (kg/kg)

(b) Precipitation efficiency and recycling in lower boundary layer: We focus on the boundary layer efficiency and recycling of precipitation over the monsoon regions on monthly scales to account for the steady state. Precipitation Efficiency (PE) is calculated as PE = P/(P+E), and the Recycling Ratio(RR) as E/P. The PE is derived from the surface moisture budget as an index of the fraction of total surface moisture flux (precipitation downward + evaporation upward) that is returned as precipitation.These simple, yet novel metrics provide preliminary insights into the processes.

Figure 10 shows that SAsiaM has the highest precipitation efficiency (~71%), followed by NAfriM (~60%) and NAmerM (~50%). The African core shows a modest but systematic increase in PE at 10 km (+2%), suggesting improved efficiency at higher resolution, likely due to better-resolved land-atmosphere coupling and convective organization. In contrast, the SAsiaM and NAmerM cores show little resolution dependence. For SAsiaM, this is likely because the large-scale monsoon circulation is so strong and moisture-rich that even coarse resolutions achieve high efficiency, leaving little room for further improvement. For North America, PE remains consistently lower (~50%) across all resolutions, possibly due to complex orography and a different convective regime that is less sensitive to resolution changes within the 80–10 km range. These regional differences indicate that the sensitivity of precipitation efficiency to resolution depends on the dominant physical processes in each monsoon core

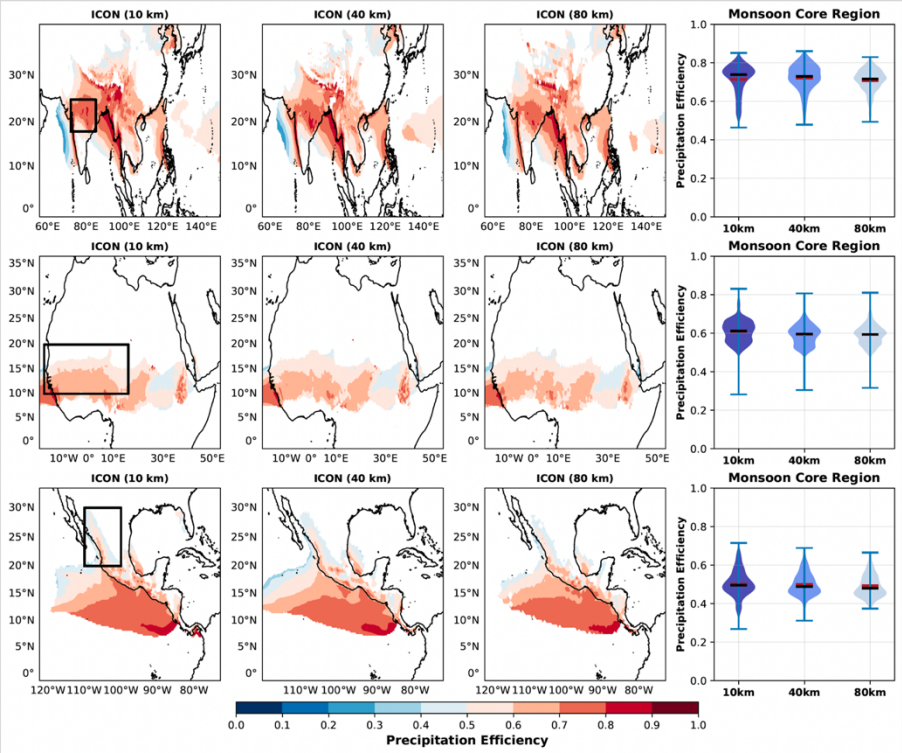

Figure 10: Sensitivity of PE to grid spacing in ICON 10 km, 40 km, and 80 km simulations for the SAsiaM, WAfriM, and NAmerM domains. The viollin plot on the right panel shows values over the respective core monsoon regions.

The recycling ratio in Fig. 11 shows that the NAfriM monsoon has the highest local moisture recycling (~70%), followed by SAsiaM (~40-45%). The NAmerM core shows RR slightly above 1, which is consistent with the inclusion of oceanic grid points (Gulf of California) where evaporation exceeds precipitation. Resolution dependence is weak overall, though the NAfriM shows a slight decrease in recycling at 10 km. Taken together, these metrics reveal a consistent picture. Overall, precipitation efficiency and recycling ratios show only modest resolution

dependence (e.g., Africa PE: +0.02, RR: -0.05). This indicates that the substantial increase in total precipitation at 10 km, particularly in the heavy tail, is not primarily due to changes in local surface moisture partitioning. Instead, the increase is driven by stronger vertical velocities (w) that accelerate the conversion of cloud water to rain water, and by increased large-scale moisture advection into the monsoon core

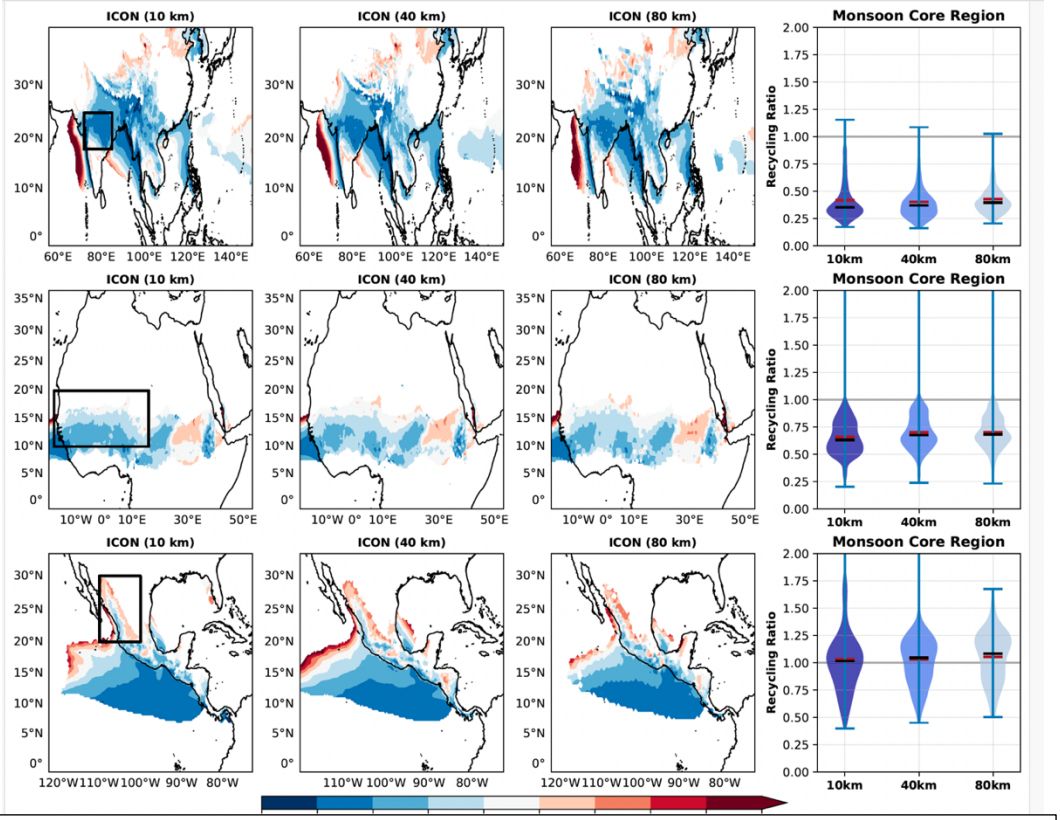

Figure 11: Same as Fig.10, but for RR.

6. The authors could provide more details on the models like what timesteps are used for the three models?

- We have provided some of the important timesteps used in the model integration in the methodology section of the submitted manuscript (L135-L137). For clarity, we provide the full details here in a table. Furthermore, we have added additional timestep information for fast-physics processes in the revised manuscript.

Table 2: Various dynamic and physics time steps used in ICON simulations

Model Parameter	ICON 10 km	ICON 40 km	ICON 80 km
Dynamical timestep	60 sec	180 sec	360 sec
Radiation scheme	360 sec	360 sec	360 sec
Cloud cover scheme	60 sec	180 sec	360 sec
Convection scheme	60 sec	180 sec	360 sec

orographic gravity wave drag (sso)	60 sec	180 sec	360 sec
non-orographic gravity wave drag (gwd)	60 sec	180 sec	360 sec
Fast-physics processes	60 sec	180 sec	360 sec

- Fast-physics include: saturation adjustment, surface transfer scheme, land-surface scheme, boundary-layer/turbulent vertical diffusion scheme, and microphysics scheme.
- In all configurations, the timestep scales approximately linearly with grid spacing, with the 10 km simulation using a 60-second dynamical timestep, while the 40 km and 80 km simulations use 180 and 360 seconds, respectively.